Robust Control Techniques for a Commercial Autoland System

JOHN L. CRASSIDIS

A robust controller, using H_∞ control design techniques, is developed for a commercial landing system. First, a detailed nonlinear aircraft computer simulation of a commercial aircraft is summarized. The computer simulation, which includes the aircraft flight dynamics, pitch attitude autopilot, and automatic thrust compensator, is presented for a Boeing 737 aircraft. The aircraft simulation is first derived by using a full 6-degree-of-freedom rigid-body model. The model is then increased to include the pitch autopilot and automatic thrust compensator. The control variables for these systems are the elevator, which generally controls pitch angle, and the thrust, which generally controls airspeed. A detailed digital computer simulation allows the replacement of simplified transfer function models for use in an autoland simulation. Therefore, internal states and dynamics associated with the aircraft subsystems can be evaluated. Then, a linear model is used to design a robust controller for the autoland process. The robustness of this controller, with respect to parameter and structural uncertainties, is tested with the aircraft simulation. The design study indicates that this controller dramatically improves the response characteristics and performance of the autoland system.

Commercial and military autoland systems have become more necessary in order to maintain busy flight schedules with safety during poor visibility or bad weather conditions. Today, both military and civil aircraft rely heavily on automatic control systems to provide artificial stabilization, with the use of autopilots to help pilots navigate and land their aircraft in bad weather. Robust control techniques, with respect to aircraft and environmental variations, in the interaction between the aircraft tracking systems and handling qualities are being investigated in the research community. With the aid of flight simulation techniques, emphasis on autoland systems could lead to the reduction of human error during the landing procedure. Therefore, the transfer of simulated robust control techniques to actual landing systems is plausible for both military and civil application in the near future.

The FAA, concerned with aviation safety, has defined specific categories of visual reference conditions with respect to pilot decision height and runway visual range. These considerations provide the basis for aircraft guidance and pilot landing procedures when visibility or weather conditions are extremely degraded (*1*). The use of the instrument landing system enables pilots to land aircraft safely in adverse weather when normal landing procedures using visual reference alone are inadequate. The instrument landing system provides pilots with glide slope information, via a localizer beam, and permits them to guide an aircraft safely through a low-visibility cloud ceiling until they can see the runway. Autoland systems expand the instrument landing system by using an aircraft's autopilot and automatic thrust compensator so that the aircraft is guided all the way to touchdown.

The aircraft's autopilot and automatic thrust compensator are essential components in a commercial autoland system. Primary components of an autoland system include a localizer beam, a glide path coupler, aircraft subsystems, and an automatic flare control system. The localizer beam is used to position the aircraft on a trajectory and intercept the centerline of the runway. The glide path coupler then calculates corrective control commands, which are transmitted to the aircraft's subsystems. The aircraft's autopilot and thrust compensator respond to these flight control commands, which indirectly control the aircraft's position and orientation. Finally, as the aircraft approaches the touchdown point the automatic flare control system is engaged, which enables a decrease in the vertical descent rate in order to allow the aircraft to land safely.

The design methodology of the current autoland system relies on classical control design techniques, such as proportional-integral (PI) control. Other areas of research and interest in the autoland process include fuzzy logic designs (*2*) and microwave landing systems (*3*). Fuzzy logic applications have demonstrated a number of benefits including improved performance, reduced power consumption, and shorter development times. One reason that fuzzy logic controllers have produced these benefits is that they easily embed human-type maneuvers into a mathematically based controller. However, because fuzzy logic depends on categorizing human responses, it may be difficult to create mathematical relations to model pilot handling qualities in an autoland system.

The microwave landing system is capable of determining the position of an aircraft over a large coverage area; therefore, it is less sensitive to surrounding interference during the autoland process. The microwave landing system also allows for increased reliability and maintainability. However, the system requires hardware changes to the current autoland system. The focus in this paper is to investigate the replacement of the current controller in the commercial landing system with a controller that is robust to surrounding interference and structural variations during the landing process. This control design requires only a software change to the current control strategy.

H_∞ methods provide new techniques and perspectives, compared with classical control techniques, in designing control systems. The frequency response characteristics of a plant are shaped according to prespecified performance specifications, in the form of weighting functions. The H_∞ design process is

Department of Mechanical and Aerospace Engineering, State University of New York at Buffalo, Buffalo, N.Y. 14260.

chosen because it (a) provides robust stability, (b) achieves performance requirements efficiently, (c) handles both disturbance attenuation and controller saturation problems easily, and (d) works not only on single-input/single-output systems, but also on complex multi-input/multi-output systems. Therefore, frequency response criteria can easily be shaped to desired specifications.

Previously, autoland simulations used a reduced linear model for the aircraft simulation (*4–7*). These models, obtained from experimental flight data, incorporate a transfer function relating the aircraft's attitude response to the transmitted pitch control command. However, the reduced models neglect the dynamic effects of the autopilot and thrust compensator. Of particular interest is the aircraft's response to atmospheric turbulence. With the transfer function model, the aircraft's response to turbulence is solely controlled by the autoland controller. But, in practice, the automatic thrust compensator also minimizes the aircraft's response to turbulence. The transfer function model approach neglects this internal control system.

In this paper, the fundamental elements and feedback control systems of the pitch autopilot and thrust compensator are shown and incorporated into a computer-generated simulation. The simulation is first presented for an open-loop study by a numerical integration scheme of the rigid-body equations of motion (the simulation is shown in the vertical-altitude plane only, although the techniques are easily extended to the horizontal plane). The closed-loop system results are shown, so that the simulation can be analyzed in order to develop a robust control design for the autoland approach simulation. Then a linearized model of the aircraft simulation is used to develop an controller for the autoland system. Finally, performance characteristics of this controller are shown in order to investigate the stability robustness and disturbance sensitivity of the control design.

DESCRIPTION OF SIMULATION

Aircraft Model

The aircraft simulation is derived by using a 12th-order state-space model, based on the 6-degree-of-freedom rigid-body aircraft dynamic equations of motion and the concept of static stability using aircraft forces and moments [see elsewhere for details (*8,9*)]. All computer simulation trajectories are produced for a Boeing 737 aircraft. Experimental (wind tunnel) aerodynamic coefficients are provided by the National Aeronautics and Space Administration (NASA) (*10*). Equation Set 1 summarizes these aircraft equations of motion.

$$\dot{p} = [-(I_{zz} - I_{yy})qr]/I_{xx} + (k_1\beta + k_2 p + k_3 r + b_1\delta_a + b_2\delta_r)0.5(\bar{V})^2$$

$$\dot{q} = [-(I_{xx} - I_{zz})pr]I_{yy} + (k_4\alpha + k_5 q + b_3\delta_e)0.5(\bar{V})^2 + b_4\bar{T}$$

$$\dot{r} = [-(I_{yy} - I_{xx})qr]I_{zz} + (k_6\beta + k_7 p + k_8 r + b_5\delta_a + b_6\delta_r)0.5(\bar{V})^2$$

$$\dot{\Phi} = p + q\sin\Phi\tan\Theta + r\cos\Phi\tan\Theta$$

$$\dot{\Theta} = q\cos\Phi - r\sin\Theta$$

$$\dot{\Psi} = (q\sin\Phi + r\cos\Phi)/\cos\Theta$$

$$\ddot{x} = [k_{10} + k_{11}\alpha + k_{12}\beta + b_7\delta_a + b_8\delta_r + b_9\delta_e]0.5(\bar{V})^2 + b_{10}\bar{T}$$

$$\ddot{y} = [k_{13} + k_{14}\alpha + k_{15}\beta + b_{11}\delta_a + b_{12}\delta_r + b_{13}\delta_e]0.5(\bar{V})^2 + b_{14}\bar{T}$$

$$\ddot{z} = [k_{16} + k_{17}\alpha + k_{18}\beta + b_{15}\delta_a + b_{16}\delta_r + b_{17}\delta_e]0.5(\bar{V})^2 + b_{18}\bar{T} + g$$

$$\dot{x} = \dot{x}$$

$$\dot{y} = \dot{y}$$

$$\dot{z} = \dot{z} \qquad (1)$$

where

α, β = angle of attack and sideslip angle;
p, q, r = angular velocities;
Φ, Θ, Ψ = roll, pitch, and yaw angles;
$\delta_e, \delta_a, \delta_r$ = elevator, aileron, and rudder angles;
$\bar{V}, \bar{T}$ = airspeed and thrust; and
$\ddot{x}, \ddot{y}, \ddot{z}$ = translational accelerations in an inertial reference frame.

The symbols $k_{i's}$ and $b_{i's}$ represent aircraft forces, moments, and other constants. [See elsewhere for more details (*9*).]

To evaluate the aircraft equations of motion for an actual aircraft trajectory, an open-loop simulation was first conducted using 737 aircraft coefficients. All trajectories are initially started with the aircraft set to trimmed values. For landing, the final approach speed is approximately 240 ft/sec (the trim values for angle of attack and elevator setting are 1.7 and -18 degrees, respectively).

Pitch Autopilot

The basic block diagram for the closed-loop system of the pitch autopilot with attitude feedback is shown in Figure 1. The pitch autopilot operates as follows. A desired pitch command is sent to the aircraft. A pitch angle error signal, representing the difference between the measured pitch angle and the desired pitch angle, is the input to the autopilot controller. The controller commands changes in the elevator setting, relative to a datum (typically, the trim value). The aircraft then responds to the new elevator setting with changes in pitch angle, pitch rate, vertical acceleration, and angle of attack.

Closing the loop using only attitude feedback achieves the desired pitch angle. But, because the aircraft has very little natural damping, the closed-loop response characteristic also has a low damping ratio. The dynamic performance of the aircraft can be severely degraded, even causing the system to become unstable. To achieve significant damping and dynamic performance, a pitch rate feedback is also provided (represented by the inner loop of the block diagram in Figure 1). The control gains used in the simulation are the gains used on an actual 737 autoland system from NASA Langley (*10*). The use of these gains helps to ensure that a proper and practical simulation is derived. Therefore, the simulation can provide a practical means of developing realizable control strategies.

The elevator controller equation in the frequency domain is given by (*10*)

$$\Delta\delta_e = \left[K_{ag}(\Theta - \Theta_c) + \frac{sK_{rg}}{s+1}\dot{\Theta}\right]\left(\frac{1+2s}{2s}\right) \qquad (2)$$

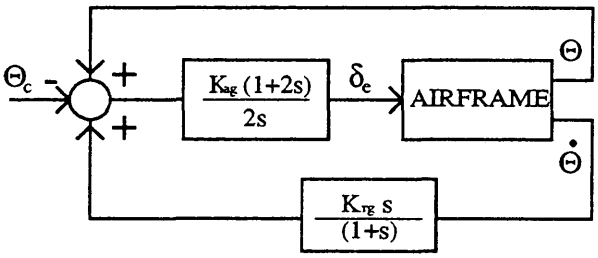

FIGURE 1 Block diagram of pitch autopilot with rate feedback.

where

s = Laplace transform variable,
K_{ag} = attitude gain,
K_{rg} = pitch rate gain, and
Θ_c = input pitch command.

The autopilot simulation is accomplished by converting the aircraft equations of motion (Equation 1) into state-space form and numerically integrating. The autopilot is engaged when the aircraft is trimmed in straight and level flight (Θ_0 = 1.7 degrees). The input to the feedback system is a pitch change command relative to the trim level. The elevator command is also implemented as a relative change from the initial setting:

$$\delta_{e_{new}} = \delta_{e_{trim}} + \Delta\delta_e \tag{3}$$

Simulation results are shown later.

Automatic Thrust Compensator

The autopilot achieves the desired pitch angle, but the inertial flight path angle (γ) must be controlled in order to land the aircraft using the autoland system. One method of achieving a desired flight path angle is to control indirectly the angle of attack to a desired reference point (e.g., the trim value) while also controlling the pitch angle, since the flight path angle represents the difference between the pitch angle and angle of attack. This control is incorporated by maintaining the aircraft's airspeed at a constant level.

The thrust compensator commands thrust changes according to the control law (*10*)

$$\Delta T_c = \left[\left(1 + \frac{K_{com}}{s}\right)\left(\frac{1}{\tau_t s + 1}\right)\left(\frac{1}{\tau_e s + 1}\right)\right]\Delta e \tag{4}$$

where

U_{ref} = reference airspeed of aircraft (usually set to level flight condition),
Δe = detected airspeed error (measured versus commanded),
ΔT_c = change in thrust commanded by autothrottle system,
K_{com} = compensator gain,
K_s = speed feedback gain,
τ_t = throttle servo time constant, and
τ_e = engine lag time constant.

These control gains and time constants used in the simulation are again from the actual 737 autoland system.

Coupling of Autopilot and Thrust Compensator

The combined closed-loop system incorporates the pitch autopilot with pitch rate feedback and the automatic thrust compensator. A pitch command is sent to the pitch autopilot. A pitch angle error signal, representing the difference between the measured and commanded pitch angles, is the input to the controller. The controller, coupled with the pitch rate feedback loop, commands changes in the elevator setting. This command is added to the trim elevator setting. The aircraft then responds to the new elevator setting, producing changes in pitch angle, pitch rate, vertical acceleration, and angle of attack. This part of the closed loop is represented by the pitch displacement autopilot with the feedback loop given by Equation 2. The autopilot also invokes a change in airspeed and angle of attack from the desired values. When this happens, the automatic thrust compensator engages, given by Equation 3, so that the airspeed and angle of attack are controlled. The autopilot and automatic thrust compensator closed-loop operation continues until the flight path angle of the aircraft is changed, which causes a change in aircraft altitude.

Simulation Results

The combined closed-loop response for a 1-degree step pitch command is shown in Figure 2. By incorporating the autopilot loop, the steady-state pitch angle error is near zero. Also, the rise time for the aircraft response is approximately 3 sec. The angle of attack response for this step input is shown in Figure 3. With the autopilot only (dashed line), the combined angle of attack and pitch angle do not enable the control of the inertial flight path angle. The thrust compensator controlled the angle of attack back to the desired trim value (the compensator can control the angle of attack to any desired setting). This combined closed loop now enables the control of the inertial flight path angle to any desired value. Therefore, the autopilot and thrust compensator simulation can be expanded to simulate the autoland process.

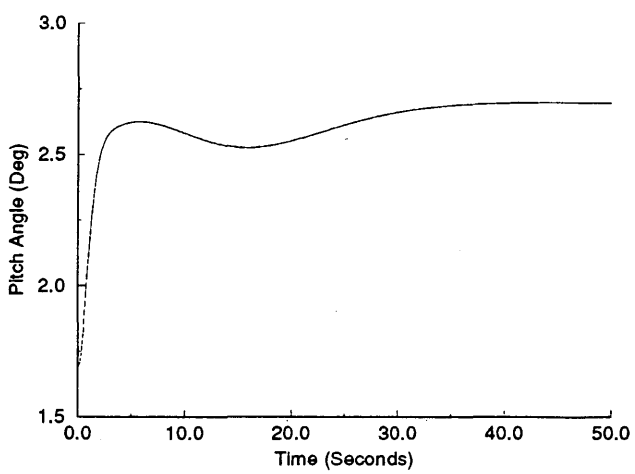

FIGURE 2 Combined closed-loop pitch angle step response.

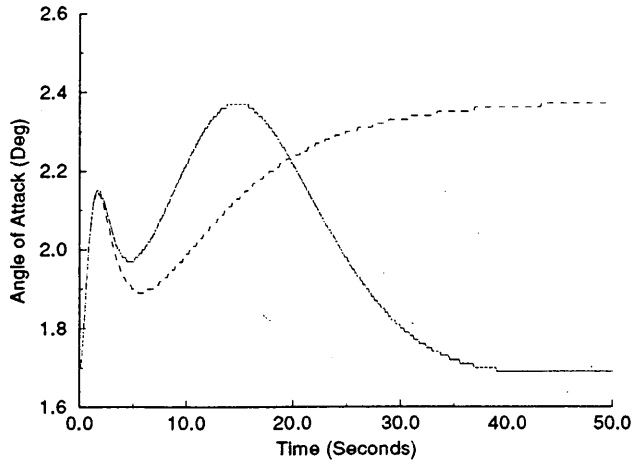

FIGURE 3 Combined closed-loop angle of attack response.

Though the aircraft model is a set of nonlinear differential equations, the response characteristics of the pitch autopilot are linear to the input command signal. This feature is illustrated in the following table, using different magnitudes for the step pitch command:

Step Pitch Command (degrees)	*Rise Time (sec)*	*Settling Time (sec)*
1	3.1	35
4	3.5	34
−3	3.6	34

The vertical acceleration closed-loop response for a 1-degree step pitch command is shown in Figure 4. The initial drop in vertical acceleration is caused by a pitching moment induced when the elevator setting is changed (i.e., a positive pitching moment causes an initial drop in vertical acceleration). The response without the automatic thrust compensator (dashed line) is lightly damped ($\zeta \approx 0.4$). But with the addition of the thrust compensator (solid line), the settling time for the system is faster because of a higher damping ratio ($\zeta \approx 0.6$). This improved acceleration characteristic also provides an increase in stability in the aircraft response to atmospheric disturbances such as turbulence. The thrust history, from the combined closed-loop response, for a step pitch command has a steady state value of 22,000 lb. Therefore, the thrust increases a net 2,200 lb from the initial level flight thrust setting (19,800 lb). This increase in thrust causes the aircraft to gain altitude. The magnitude of the airspeed response is not significantly changed, which is ideal for the automatic landing process.

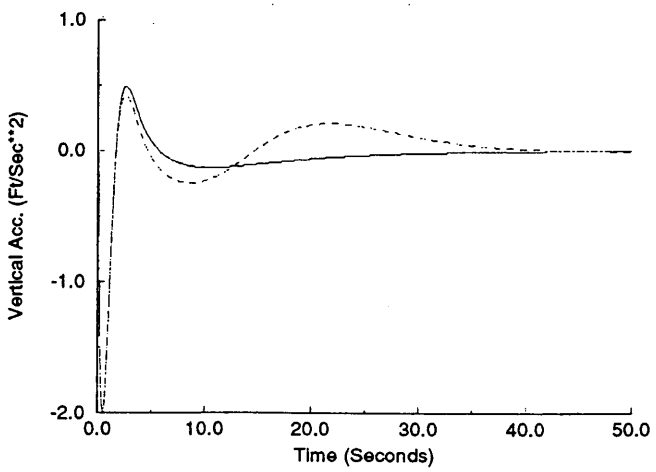

FIGURE 4 Closed-loop vertical acceleration response.

ATMOSPHERIC TURBULENCE

The stochastic process of atmospheric turbulence is summarized in this section. Turbulence is a result of instabilities in the velocity field of the atmosphere. The instabilities are caused by such things as solar heating or the earth's rotation; they give rise to gradients in temperature, pressure, and velocity (*9*). Turbulence is random in nature and, in the longitudinal plane, is characterized by horizontal and vertical wind gusts. The horizontal gusts affect the aircraft's altitude by changing the airspeed of the aircraft, which varies the lift on the airplane's wings and causes the aircraft to rise or fall, depending on whether the wind gusts add or subtract from the aircraft's nominal airspeed. Similarly, vertical gusts vary the angle of attack of the aircraft, which also results in a change in the aircraft's altitude.

Because of the complicated and changing nature of turbulence, some simplifying assumptions must be made to develop a model that can be realized mathematically (*11*). First, the turbulence is assumed to be locally isotropic. Isotropy refers to the independence of the statistical properties of the turbulence on the orientation of the coordinate axes. Second, the turbulence is assumed to be homogeneous, implying that all of the statistical properties are the same at each point in the velocity field. A result of these assumptions is that the horizontal and vertical wind velocities will have a small effect on each other, or in mathematical terms, a low cross correlation. Therefore, the aircraft's response to horizontal and vertical wind gusts can be separated individually. Because of the similarity of the two responses, only one of these responses needs to be analyzed. For these reasons, only the effects of the longitudinal wind gusts on the aircraft's vertical velocity are considered as turbulence input.

The aerodynamic forces and moments acting on the aircraft depend on the relative motion of the aircraft to the atmosphere and not on the inertial velocities. Therefore, to account for atmospheric gusts, the forces and moments must be related to the relative motion with respect to the atmosphere. This is accomplished by expressing the velocities used in calculating the aerodynamics in terms of inertial and gust velocities:

$$\Delta u_a = \Delta u - u_g$$

$$\Delta v_a = \Delta v - v_g$$

$$\Delta w_a = \Delta w - w_g \tag{5}$$

where u_g, v_g, and w_g are gust velocities in the X, Y, and Z directions, and the Δ-quantities are the perturbations in the inertial velocity variables.

Two spectral forms of random continuous turbulence are generally used to model atmospheric turbulence for aircraft response studies. They are the mathematical models named after Von Karman and Dryden, the scientists who first proposed them.

The Von Karman model shows that the power spectral density approaches a constant value asymptotically at low frequencies and decreases asymptotically according to a $-5/3$ power frequency for higher frequencies (*9*). These high frequencies occur in a range called the inertial subrange, in which energy is neither fed into nor dissipated from the turbulence. Mathematically, this relationship can be expressed by

$$\Phi_{u_g}(\Omega) = \sigma_u^2 \frac{2L_u}{\pi} \frac{1}{[1 + (1.339L_u\Omega)^2]^{5/6}}$$

$$\Phi_{v_g}(\Omega) = \sigma_v^2 \frac{2L_v}{\pi} \frac{1 + 8/3(1.339L_v\Omega)^2}{[1 + (1.339L_v\Omega)^2]^{11/6}}$$

$$\Phi_{w_g}(\Omega) = \sigma_w^2 \frac{2L_w}{\pi} \frac{1 + 8/3(1.339L_w\Omega)^2}{[1 + (1.339L_w\Omega)^2]^{11/6}} \tag{6}$$

where

Φ = dimensional power spectrum,
σ = root-mean-square intensity of gust component,
Ω = spatial frequency, and
L = scale of turbulence.

The wavenumber Ω can be converted from a spatial wavelength to a temporal frequency by multiplying the wavenumber by the aircraft's airspeed $\bar{V}$ as follows: $\omega = \Omega \bar{V}$.

The scale of turbulence for clean air turbulence is defined as follows (*9*):

$$\text{Above } z = 2{,}500 \text{ ft}, \quad L_{wg} = 2{,}500$$

$$\text{Below } z = 2{,}500 \text{ ft}, \quad L_{wg} = 184(z)^{1/3} \tag{7}$$

For an aircraft landing, the altitude z varies as the aircraft descends. Because of the way in which the power spectral density of the turbulence is defined in the Von Karman model, the corner frequency of the turbulence increases as the aircraft descends. For the turbulence conditions likely to be encountered by the aircraft landing, a range of corner temporal frequencies from 0.5 to 1.0 rad/sec is used. Several data sets of turbulence are used in the simulation in order to investigate the response characteristics of the aircraft.

Robust Control Design

The aircraft simulation can now be used to investigate the feasibility of a robust (H_∞) control design for the automatic landing approach. A block diagram of the glide slope intercept and hold system is shown in Figure 5. The glide slope receiver in the aircraft is designed to sense the angular Γ error relative to the glide slope of the station. This signal is compared to the desired glide slope error Γ_{ref} introduced into the closed-loop system. An error signal is produced that is sent to the controller/coupler. The controller network then generates a pitch command that is transmitted to the aircraft's autopilot and thrust compensator. The aircraft responds to this pitch command as previously described, so that the aircraft's altitude changes with a change in flight path angle. This closed-loop operation continues until the aircraft lands on the landing strip.

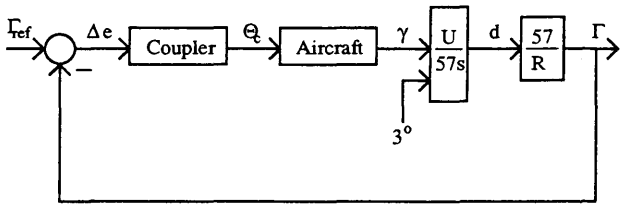

FIGURE 5 Block diagram of autoland system.

The design of robust controllers has been investigated extensively over the past decade (*13–15*). The next step is to develop an H_∞ control design for the coupler while attenuating the turbulence response of the aircraft. The H_∞ criterion is chosen because robust stability in the closed-loop system can be achieved easily by defining performance and robustness specifications in the form of weighting functions. In this manner, frequency response criteria in the autoland system are shaped to desired specifications.

The H_∞ criterion, with controller $K(s)$ and plant $G(s)$, considers the closed-loop system performance on disturbance sensitivity $S(s)$ and stability $[I - S(s)]$ to prespecified weighting functions, denoted as $\gamma W_1^{-1}(j\omega)$ and $W_2(j\omega)$, respectively. The requirements for stability and disturbance attenuation are specified in terms of singular value inequalities (*13*):

$$\bar{\sigma}[S(j\omega)] \leq |W_1^{-1}(j\omega)|$$

$$\bar{\sigma}[I - S(j\omega)] \leq |W_2(j\omega)| \tag{8}$$

where $\bar{\sigma}$ represents the maximum singular value. These specifications are combined into a single infinity norm:

$$\left\| \begin{matrix} W_1 S \\ W_2(I - S) \end{matrix} \right\|_\infty \leq \gamma \tag{9}$$

This equation shapes the frequency loop transfer function $[L(s) = G(s)K(s)]$ by penalizing the sensitivity function $[S = (I + GK)^{-1}]$ to reject the plant disturbances (turbulence), and high frequency $L(s)$ by penalizing the complementary sensitivity function $[T = GK(I + GK)^{-1}]$ to cope with model uncertainties—for example, unmodeled (high-order) dynamics, sensor and actuator dynamics, and so on (*13*). The solution of Equation 9 involves an iteration on the γ term of the specified disturbance weighting function. As γ is increased, the sensitivity function S decreases and the complementary sensitivity function $(I - S)$ approaches the W_2^{-1} weight. Therefore, the function in Equation 9 approaches its zero-decibel limit. The controller solution is determined by a two-Riccati solution (*15*).

Linear Model

The combined computer simulation of the 12th-order aircraft model, pitch attitude autopilot, and thrust compensator results in a complex (high-order) model. A state-space model between the pitch command input and the aircraft flight path angle output can be obtained by linearizing the nonlinear equations of motion and creating closed-loop transfer functions for each feedback loop; however, this involves extensive

computational time. To develop a linear model, time-domain techniques are used instead to obtain pole/zero locations of the aircraft, autopilot, and thrust compensator. Therefore, the input/output relationship of the aircraft can accurately be obtained. And time-domain techniques are more realistic, since operational data can be used in the design process.

Several identification techniques have been derived for developing accurate model realizations from time-domain data (*16–18*). The technique used in the aircraft realization is the Eigensystem realization algorithm (ERA) (*18*). The ERA method is chosen because (a) only discrete, time-domain impulse response data are required; (b) the computational requirement is relatively easy; (c) the numerical stability properties have internally balanced realizations; and (d) accurate model representations are possible if the discrete measurements are of low noise in nature. Therefore, a mathematical model of the system is constructed, reproducing the plant's input/output behavior. A complete derivation of the ERA method can be found elsewhere (*18*). This algorithm produced an 18th-order realization of the 737 aircraft and autopilot simulation.

Because of computer software and hardware requirements, the robust control design requires the need for reduced plant models. This need arises because the H_∞ control design results in a controller's having a degree of at least the same order as the plant, that is, 18th-order. Therefore, a model reduction is essential in developing a realizable control strategy. The Schur balanced model reduction technique is used to develop a reduced fifth-order model (*19*). This model is determined as

$$\frac{Z(s)}{\Theta_c(s)} = \frac{0.083s^5 + 0.52s^4 + 1.55s^3 - 0.52s^2 + 0.08s + 0.006}{s(s^4 + 1.06s^3 + 0.75s^2 + 0.0388s + 0.02)} \quad (10)$$

where $Z(s)$ is the altitude of the aircraft. The aircraft model, pitch autopilot, and thrust compensator have a flight path response bandwidth of approximately 1 rad/sec, which is required to achieve good glide slope control for an aircraft under autoland control.

Control Design Results

The robust control design is developed using the reduced-order model given by Equation 10. When the final design is complete, the controller is incorporated into the full aircraft, autopilot, and thrust compensator simulation, given Equations 1 through 4. This adds to the validity for the use of the reduced model in the H_∞ design process.

The complementary sensitivity function is weighted using a first-order weighting function. This weighting function is chosen to achieve the fastest possible response time in the closed-loop system while maintaining the control and actuator limitations in the aircraft response characteristics. The optimal control design achieves a bandwidth specification for the closed-loop system of about 1.8 rad/sec with no overshoot. The sensitivity function is weighted such that the disturbance responses to turbulence are attenuated at least 500:1 with a first-order roll-off of 1 rad/sec. The design specifications obtain the maximum bandwidth response possible, subject to minimizing the sensitivity function. The combination of the sensitivity and complementary sensitivity function responses are also within controller tolerances—that is, ±10 degrees in the pitch command. Stability robustness in the presence of model uncertainties is essential for a modern control design system. In most circumstances, the mathematical model of the plant only approximately represents the behavior of the true system. The difference between the actual system and the mathematical model of the plant arises from parameter variations, unmodeled dynamics, or nonlinearities in the true system. The model error uncertainties are generally represented in terms of both additive and multiplicative uncertainty bounds (*14*). The maximum allowable additive and multiplicative plant perturbations are given by $1/\overline{\sigma}\,[K(I + GK)^{-1}]$ and $1/\overline{\sigma}[GK(I + GK)^{-1}]$, respectively. The minimum additive and multiplicative uncertainty upper bounds for this robust control design are -0.52 and -0.03 decibels, respectively. This means that even if the modeled plant has both -0.52 decibels additive uncertainty and -0.03 decibels multiplicative uncertainty at any frequency, the closed-loop system remains stable. This stability robustness property is one of the advantages of the H_∞ controller.

To demonstrate the stability robustness properties of the H_∞ controller, a comparison is made with respect to a classical control design. The current control design for the autoland land system incorporates a PI control philosophy (*10*). The control gains for the classical PI control strategy are determined from a parameter optimization scheme. The performance criterion for the classical design is evaluated with respect to optimal step response, turbulence attenuation, and controller limitations. The combination of these criteria describes the optimal closed-loop performance.

The cost function chosen for the classical PI control design is based on the integral of the error signal. A quadratic form, the integral-squared error, is used to ensure a well-defined minimum. The step response is used to evaluate the aircraft's response to a step input signal. The step response cost function is chosen as

$$\Upsilon_s = \int_{t_0}^{t_f} t\,[zer^2(t)]dt \quad (11)$$

where *zer* is the error between the desired and actual flight path angles. The turbulence response cost function minimizes the error between the desired and actual altitudes of the aircraft. The desired altitude for the turbulence response is set to zero. This cost function is given as

$$\Upsilon_t = \int_{t_0}^{t_f} [Z^2(t)]dt \quad (12)$$

where Z is the altitude of the aircraft. The final cost function minimizes the control signal level and maintains controller tolerances to within prespecified tolerances. This cost function is given as

$$\Upsilon_c = \int_{t_0}^{t_f} [\Theta_c^2(t)]dt \quad (13)$$

Optimization of any one cost function produces an optimal response for that characteristic but a degradation of other

characteristics. Therefore, a combined cost function is used. This cost function is defined as

$$Y = J_1 Y_s + J_2 Y_t + J_3 Y_c \tag{14}$$

Selection of the weights ($J_1 - J_3$) can be varied in order to trade off individual response characteristics for the classical PI control design.

Optimization Results and Comparison

A turbulence comparison plot of the robust H_∞ control design and the optimized classical PI control design is shown in Figure 6. Clearly, the turbulence response is attenuated to a higher degree with the use of the robust control design. The optimized step response comparison plot is shown in Figure 7. The robust control design has a faster time to peak and no overshoot, whereas the optimized classical control design responds slower and has a slight overshoot. These results clearly show an improvement in system performance when the robust control design is used.

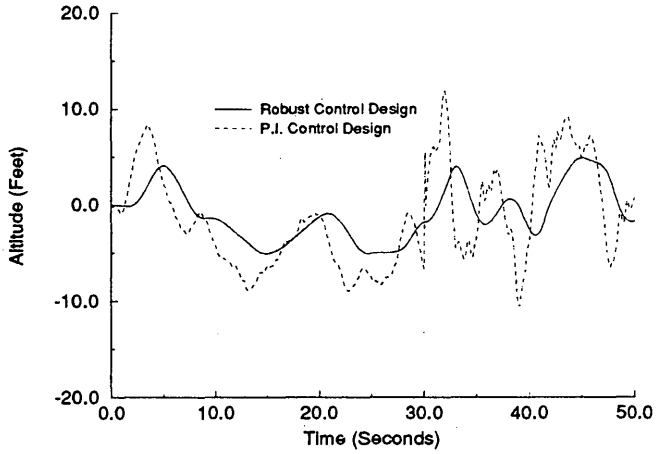

FIGURE 6 Turbulence response comparison.

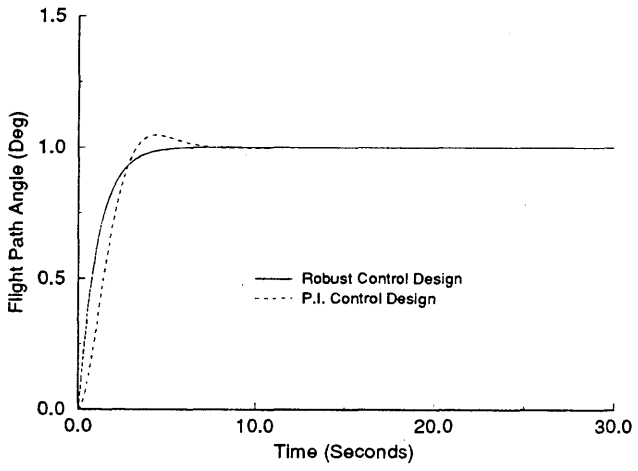

FIGURE 7 Step response comparison.

The robust control design provides better performance characteristics than the "current" classical PI control design. However, the main advantage of the H_∞ control design is the stability robustness in the presence of model uncertainties. To demonstrate this characteristic, a model error is introduced into the aircraft simulation. The model is perturbed by varying all the aircraft stability and control derivatives, given by Equation 1, by a factor of approximately 10 percent. Then both the robust control design and PI control design are compared using the perturbed plant model. Figure 8 shows the step response comparison using the model error plant. The classical PI control design is now unstable, but the robust control design remains stable. Therefore, the H_∞ control design provides a way to guarantee stability in the presence of significant model error and uncertainty.

CONCLUSIONS

In this paper, a detailed simulation of a Boeing 737 aircraft with a pitch autopilot and thrust compensator has been presented. This system was first developed with an open-loop simulation of an aircraft using a 12th-order state-space model. Then a closed-loop simulation was developed for the aircraft under autopilot and thrust compensator control. The autopilot maintains a desired pitch attitude, and the automatic thrust compensator maintains the desired airspeed and angle of attack. The combination of these systems is essential for an automatic flight path control landing.

Next, the turbulence model, used as a disturbance input to the aircraft, was summarized. Therefore, the use of the aircraft simulation and turbulence model enabled the design of a robust H_∞ controller. Combined cost functional results indicate that the robust control design attenuates the turbulence response of the aircraft by a factor nearly two times, as compared with the current controller. The new design was also robust in the presence of model and structural uncertainties.

Finally, the new control design requires only a software modification to the current landing system, so that the controller can easily be implemented onto the actual system. Therefore, an optimal design can be used to simulate an au-

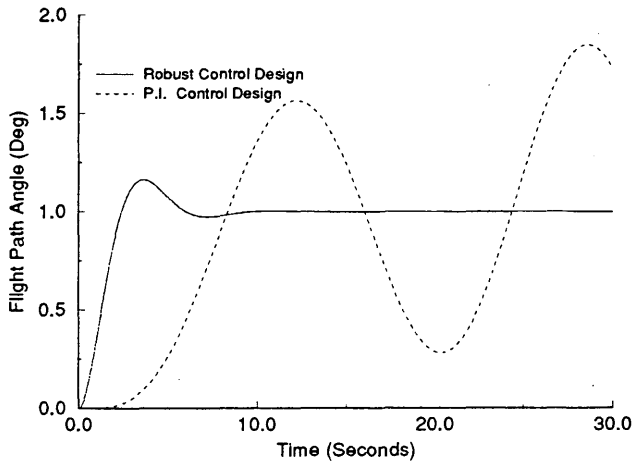

FIGURE 8 Step response comparison with perturbed plant.

tomatic aircraft landing while minimizing the adverse effects of turbulence.

ACKNOWLEDGMENTS

The research in this paper was supported by a grant provided by the FAA and administered by TRB as part of the Graduate Research Award Program on Public-Sector Aviation Issues. The author would like to thank academic advisor D. Joseph Mook, associate professor of mechanical and aerospace engineering at the State University of New York at Buffalo; TRB program coordinators Larry L. Jenney and E. Thomas Burnard; and TRB monitors R. John Hansman, associate professor of aerospace engineering at the Massachusetts Institute of Technology, and Agam N. Sinha, department head, MITRE Corporation, for their invaluable help, guidance, and encouragement in monitoring this project. Special thanks are expressed to Richard M. Hueschen of the Aircraft Guidance and Controls Branch, NASA, for providing the system parameters used in the underlying computer aircraft simulation.

REFERENCES

1. W. J. Rohling. Flying Qualities: An Integral Part of a Stability Augmentation System. Presented at the American Institute of Aeronautics and Astronautics Fifth Annual Meeting and Technical Display, Oct. 1968.
2. M. Steingerg. A Fuzzy Logic-Based F/A-18 Automatic Carrier Landing System. *Proc., American Institute of Aeronautics and Astronautics Guidance, Navigation, and Control Conference*, Aug. 1992, Paper 92-4392, pp. 407–417.
3. J. N. Barrer and A. N. Sinha. An Operational Perspective of Potential Benefits of Microwave Landing Systems. *Proc., 31st Annual Meeting of the Air Traffic Control Association*, Arlington, Va., 1986.
4. K. Kamoner and R. Benson. Design of an Integrated Autopilot/Autothrottle for NASA TSRV Airplane Using Integral LQG Methodology. *Proc., American Institute of Aeronautics and Astronautics Guidance, Navigation, and Control Conference*, Aug. 1989, Paper 89-3495, pp. 1373–1391.
5. Y. Miyazawa. Robust Flight Path Control System Design with Multiple Delay Model Approach. *Proc., American Institute of Aeronautics and Astronautics Guidance, Navigation, and Control Conference*, Aug. 1992, Paper 92-2671, pp. 642–652.
6. P. Voulgaris and L. Valavani. High Performance H_2 and H_∞ Designs for the Super Maneuverable F18/HARV Fighter Aircraft. *Proc., American Institute of Aeronautics and Astronautics Guidance, Navigation, and Control Conference*, Aug. 1989, Paper 89-3456, pp. 37–44.
7. M. J. Roemer. Robust Tracking and Control Strategies for Automatic Landing Systems. In *Transportation Research Record 1257*, TRB, National Research Council, Washington, D.C., 1990, pp. 30–43.
8. R. C. Nelson. *Flight Stability and Automatic Control*. McGraw-Hill, New York, N.Y., 1987.
9. J. Roskam. *Airplane Flight Dynamics and Automatic Control*, Parts 1 and 2. Roskam Aviation and Engineering Corp.; University of Kansas, Lawrence, 1979.
10. *Stability Derivatives, Autopilot, and Thrust Compensator Data for the ATOPS Boeing 737 Aircraft*. Report TCV-B737. National Aeronautics and Space Administration.
11. J. L. Lumley and H. A. Panofsky. *The Structure of Atmospheric Turbulence*. Interscience, New York, N.Y., 1964.
12. J. C. Houbolt, R. Steiner, and K. G. Pratt. *Dynamic Response of Airplanes to Atmospheric Turbulence Including Flight Data on Input and Response*. Report NASA TR-R-199. National Aeronautics and Space Administration, June 1964.
13. B. A. Francis, J. W. Helton, and G. Zames. H_∞ Optimal Feedback Controllers for Linear Multivariable Systems. *IEEE Transactions on Automatic Control*, Vol. AC-29, Oct. 1984, pp. 888–900.
14. B. A. Francis and J. C. Doyle. Linear Control Theory with an H_∞ Optimally Criterion. *Society of Industrial and Applied Mathematics Journal of Control Optimization*, Vol. 25, 1987, pp. 815–844.
15. J. C. Doyle, P. P. Khargonekar, and B. A. Francis. State-Space Solutions to Standard H_2 and H_∞ Control Problems. *IEEE Transactions on Automatic Control*, Vol. AC-34, Aug. 1984, pp. 831–847.
16. S. R. Ibrahim and E. C. Mikulcik. A Method for the Direct Identification of Vibration Parameters from the Free Response. *Shock and Vibration Bulletin*, No. 47, Part 4, Sept. 1977, pp. 183–198.
17. F.-B. Yeh and C.-D. Yang. New Time-Identification Technique. *American Institute of Aeronautics and Astronautics Journal of Guidance, Control, and Dynamics*, Vol. 8, No. 4, July–Aug. 1987, pp. 463–470.
18. J. N. Juang and R. S. Pappa. An Eigensystem Realization Algorithm for Modal Parameter Identification and Model Reduction. *American Institute of Aeronautics and Astronautics Journal of Guidance, Control, and Dynamics*. Vol. 8, No. 5, Sept–Oct. 1985, pp. 620–627.
19. M. G. Safonov and R. Y. Chiang. Model Reduction for Robust Control: A Schur Relative Error Method. *International Journal of Adaptive Control and Signal Processing*, Vol. 2, 1988, pp. 259–272.
20. J. M. Urnes and R. K. Hess. Development of the F/A-18A Automatic Carrier Landing System. *American Institute of Aeronautics and Astronautics Journal of Guidance, Control, and Dynamics*, Vol. 8, No. 3, May–June 1985, pp. 289–295.
21. J. M. Urnes, R. K. Hess, R. F. Moomaw, and R. W. Huff. H-Dot Automatic Carrier Landing System for Approach Control in Turbulence. *American Institute of Aeronautics and Astronautics Journal of Guidance, Control, and Dynamics*, Vol. 4, No. 2, March–April 1981, pp. 177–183.
22. C. T. Villarreal. Uses and Misuses of Risk Metrics in Air Transportation. In *Transportation Research Record 1161*, TRB, National Research Council, Washington, D.C., 1988, pp. 31–42.
23. J. L. Crassidis, D. J. Mook, and J. McGrath. An Automatic Carrier Landing System Utilizing Aircraft Sensors. *American Institute of Aeronautics and Astronautics Journal of Guidance, Control, and Dynamics* (in preparation).
24. J. L. Loeb. Automatic Landing Systems Are Here. *Proc., Advisory Group for Aerospace Research and Development Conference on Aircraft Landing Systems*, No. 59, 1969.
25. D. J. Sheftel. New Guidance Development for All Weather Landing. *Proc., Advisory Group for Aerospace Research and Development Conference on Aircraft Landing Systems*, No. 59, 1969.